Water Science & Technology

IWA PUBLISHING

Water Science & Technology Vol 87 No 8, 1969 doi: 10.2166/wst.2023.106

On-site performance evaluation of a 1,000-litre microbial fuel cell system using submergible multi-electrode modules with air-cathodes for sustainable municipal wastewater treatment and electricity generation

J. Heinrichmeier [a,*], Tobias Littfinski[a,b], Ekaterina Vasyukova[a], Leon Steuernagel[a] and Marc Wichern[b]

[a] WTE Wassertechnik GmbH, Ruhrallee 185, 45136 Essen, Germany
[b] Department of Civil and Environmental Engineering, Institute of Urban Water Management and Environmental Engineering, Ruhr-Universität Bochum, Universitätsstraße 150, 44780 Bochum, Germany
*Corresponding author. E-mail: juergen.heinrichmeier@wte.de

JH, 0000-0002-4232-1772

ABSTRACT

The reliability of a microbial fuel cell (MFC) system was tested on an industrial scale by operating a 1,000-L single-chamber system under real conditions at a municipal wastewater treatment plant (WWTP) over a 6-month period. Submergible multi-electrode modules with large-scale grid-segmented gas diffusion cathodes with activated carbon as a catalyst were used. Maximum power densities normalised to the cathode area were above 100 mW m_{Cat}^{-2}. Fluctuating chemical and physical wastewater characteristics of the influent had reversible effects on MFC performance in terms of energetic efficiency. Thereby, the composition of the chemical oxygen demand (COD) fractions changes only insignificantly and the concentration of readily biodegradable (S_S) required for the enhanced biological phosphorus removal (EBPR) process or upstream denitrification was reduced by 41 $\pm$ 10 mg L^{-1} (37 $\pm$ 2% of inflow S_S).

Key words: 1000-L microbial fuel cell, COD fractionation, large-scale air-cathodes, long-term operation, municipal wastewater, submerged multi-electrode modules

HIGHLIGHTS

- A 1,000-L air-cathode microbial fuel cell (MFC) reactor was operated over a 6-month period in a municipal wastewater stream.
- Large-scale raster segmented air-cathodes in submersible modules for retrofit into primary settling tanks.
- Determination of COD fraction changes by MFC prior to EBPR and upstream denitrification.
- Evaluation of rain weather influence on MFC performance and recovery.

GRAPHICAL ABSTRACT

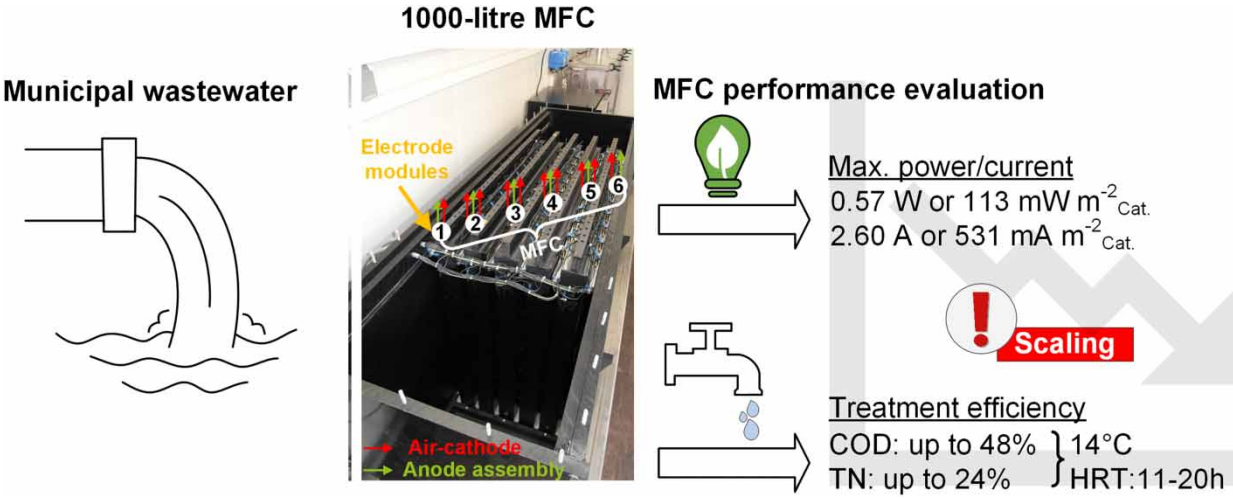

INTRODUCTION

Microbial fuel cells (MFCs) are bio-electrochemical systems with the ability to utilise microbial metabolism for the direct conversion of chemical energy to electrical energy. The model idea of biofilms harbouring exoelectrogenic bacteria can be used to describe the oxidation of organic substances under anaerobic conditions. During this biotransformation, electrons are delivered to the anode, while protons and by-products are released into the solution. Due to a theoretical maximal potential gradient of $\leq$1.105 V between an anaerobic anode (−0.30 V vs. standard hydrogen electrode, SHE) and an aerobic cathode (+0.805 V vs. SHE), the electrons are transported through an external circuit with an applied electrical load resistance to the cathode. With the help of a catalyst, they are reduced to the water together with oxygen and protons (Logan 2008).

When using municipal wastewater as feedstock, mixed microbial cultures are present in the anaerobic environment of the anodes as well as in locally aerobic zones near the air-cathode. Predictions of a whole-cell dynamic simulation model suggest not only the conversion of organic substrate. The total ammonia nitrogen (TAN) chiefly takes place via two processes: biological nitrification-denitrification and electrochemical ammonia stripping associated with a pH increase (up to 12) caused by the proton consumption at the cathode (Littfinski *et al.* 2021a). Besides the high pH near the cathode surface, the electric field favours salt precipitation at the catalyst and the gas diffusion layer. Its prevention is one of the key challenges for achieving stable long-term microbial fuel cell (MFC) performance. Rossi *et al.* (2019a) and Hiegemann *et al.* (2019) reported an energetic performance decrease of 78 and 50% after 1 month of operation using similarly activated carbon catalyst air-cathodes. The reduced area of open pores and coating of the catalyst leads to an ongoing decrease in the overall mass transfer coefficient (Littfinski *et al.* 2022).

The addressed high potential of MFCs as a sustainable wastewater treatment technology reported in the literature is mostly based on bench-scale experiments. To date, only a few published scientific research studies have been found that have investigated a MFC system with more anolyte liquid volume than 500 L (Bird *et al.* 2022; Rossi *et al.* 2022). Each of them is different in design, indicating that the MFC technology for full-stream treatment is still in the 'proof of concept' phase for municipal wastewater treatment. Among these six studies, there are only two pilot studies (including this study, see Table 1) in which large-scale air-cathodes were used. Thus, further pilot studies like this presented one are essential to evaluate and demonstrate the design feasibility with deeper submerged hydrophilic air-membranes, their performance and influence on following biological treatment steps depending on the readily biodegradable organic substrate, as well as specific scaling-up challenges before a reliable full-scale evaluation of the technical and economic viability can be done (Wang & He 2020; Bird *et al.* 2022).

When scaling-up MFCs, the need for a high electrode packing density is one of the major tasks to achieve a comparable energetic and treatment performance as in bench-scale. For example, the characteristic polarisation curve (cell voltage and/or electrode potential as a function of current density) of an ideal MFC is not only a result of the installed materials and the designed system but is also linked to the electrode's surface area and electric capacitance. Electrochemical losses

Table 1 | List of comparable pilot studies using air-cathodes reported in the literature

	Rossi *et al.* (2019b)	Babanova *et al.* (2020)	Hiegemann *et al.* (2019)	Rossi *et al.* (2022)	This study
Operation time	122 days*	>200 days	98 days*	180 days*	180 days
MFC classification					
Configuration	Single	Single (Stack)	Single	Single	Single
Reactor/module shape	Box	Box	Flat	Flat	Flat
Installation method	Chamber	Chamber	Submerged	Submerged	Submerged
Operating mode	Fed-batch	Continuous	Continuous	Continuous	Continuous
Type of wastewater	Municipal	Swine	Municipal	Municipal	Municipal
Reactor architecture					
Reactor volume (L)	85	110	255	1,400	1,000
Anode material[a] (anode surface)	22 × GFB (2.24 m^2)*	240 × GFB (2.12 m^2)*	20 × GFB (4.2 m^2)	680 × GFB (33 m^2)*	60 × GFB (9.4 m^2)
Cathode material[b] (cathode surface)	1 × SS/AC (0.486 m^2)*	Gas diffusion cathode (0.88 m^2)	2 × SS/AC (1.04 m^2)	32 × SS/AC (15 m^2)	10 × SS/AC (5.15 m^2)
Performance evaluation parameter					
$\eta_{COD,eli}$ (%)	75–80	65	25–42	49 ± 15	34 ± 7
max. PD[c] (mW m_{Cat}^{-2})	106*	84–105	78	95*	113

Note: The specified electrode area is referred to as the cylinder-equivalent surface area (anode) or the catalytically active surface area (cathode).
Calculated values are marked with *.
[a]GFB, graphite fibre brush.
[b]SS/AC, stainless steel/activated carbon.
[c]Power density.

are also dynamically dominated during operation by thermodynamic, side reaction, activation, ohmic, concentration, and turnover kinetic losses (Harnisch & Schröder 2010). For instance, substrate concentration, liquid temperature, or electrical conductivity (EC) influenced by rainfall events in mixed sewer systems also affect cell performance due to changes in cell internal parameters (Hiegemann *et al.* 2016; Adekunle *et al.* 2019; Littfinski *et al.* 2022). In municipal wastewater, these operational parameters can be subject to high fluctuations, which is why the application of real-time maximum power point tracking (Littfinski *et al.* 2021b) methods (e.g., perturbation and observation, P/O, algorithm) is inevitable to adjust the external resistance to the actual cell internal resistance of the system. According to Woodward *et al.* (2010), more than 50% of power may be lost if the external resistance does not match the internal one.

Considering the status of MFC development, a full-scale integration in municipal wastewater systems upstream from the biological wastewater treatment seems a promising challenge (Tan *et al.* 2021). Single-chamber modules, enclosing the air side of the cathodes in a watertight housing, can be submersed in wastewater tanks or for example, close to the effluent channel of primary settling tanks. To gain a more active surface, the module size can be increased by increasing the submersion depth into the settling tank. The further presented study addresses this module concept of parallel connected cells. In addition, the organic substrate degradation of the MFC is described in terms of the chemical oxygen demand (COD) fractions. The influence of the MFC system on the essential downstream activated sludge units using enhanced biological phosphorus removal (EBPR) and upstream denitrification can be determined in the context of the reduced fast-degradable COD fraction.

MATERIALS AND METHODS

MFC integration into municipal wastewater treatment plants

In this study, one of the largest ever operated pilot-scale MFC systems using multi-electrode submergible MFC modules was retrofitted between the mechanical treatment (screens, aerated grit, and grease chambers) and the activated sludge unit of an existing 40,000 peoples equivalents municipal wastewater treatment plant (WWTP) situated in Hecklingen, Saxony-Anhalt

(Germany). The MFC was continuously operated with real municipal wastewater (effluent of the primary sedimentation) over a 6-month period. The feed water volume followed a fixed dry weather diurnal variation pattern. Storm-water events are considered only by reduced wastewater concentrations. Throughout the experiments, the long-term performance stability of the MFC system was evaluated using energetic and pollutant removal efficiency measures. To restore cathode performance, the effects of acid treatment were evaluated.

Reactor and electrode module architecture

Submergible multi-electrode MFC modules formed the basic concept for the scale-up application. Ten raster segmented air-cathodes (85 cm × 85 cm; VITO NV, Belgium), mounted on five submergible modules, were placed inside a 1,000-L tank reactor (Figure 1(a)). Each cathode consisted of 16 fields of VitoCORE® electrodes (VITO NV, Belgium; 17 cm × 17 cm) with polytetrafluoroethylene (PTFE) diffusion membranes as the diffusion layer, activated carbon as the catalyst layer, and stainless steel mesh as the current collector. The total catalytically active area was 5.15 m^2_{Cat}. The approximately 3 cm thick, air-filled part of each module was equipped with a programmable peristaltic pump (Jecod Auto Dosing Pump DP-3; Jebao, Canada) for the ongoing removal of condensate and possible leakage water.

Six anode assemblies, each consisting of 10 graphite fibre brushes (MILL-ROSE Company, USA; Ø 6 cm; 80 cm), were placed parallel to the cathodes. Due to the small distance, the anode assemblies were electrically separated by a glass fibre mat (300 g m^{-2}) as an additional layer on the current collector of the cathodes. All brushes were heat-treated at 450 °C for 30 min (Feng *et al.* 2010). The brushes were installed in 8 cm distance in the wastewater flow direction. Because the brushes touched the glass fibre separator on each side, the installation height between each brush was alternately shifted by 5 cm within the aluminium support. This created an open flow channel (Figure 1(b)) in case the anode biofilm overgrew the brushes. The total cylinder-equivalent surface area of the six anodes was 9.36 m^2_{An}. One anode assembly (1.56 m^2_{An}) and one cathode (0.515 m^2_{Cat}) formed the outer electrical Circuits 1 (MFC-1) and 6 (MFC-6). The remaining inner electrical Circuits 2–5 (MFC-2, MFC-3, MFC-4, and MFC-5) shared one anode assembly (1.56 m^2_{An}) and two parallel connected cathodes (1.03 m^2_{Cat}). This configuration allowed for six separately installed parallel electrical circuits (Figure 1(c)).

An adjustable, externally located recirculation pump (AquaForte DM-Vario 10,000, SIBO Fluidra, the Netherlands) prevents concentration gradients between bulk-liquid and electrodes and increase the mass transfer of protons. The MFC-internal recirculation flow was designed based on a chosen flow velocity over the biofilm of a minimum of 5 cm s^{-1} (Hille *et al.* 2009) for the area of this open flow channel and set to 3 m^3 h^{-1} or three times per hour gross volume exchange rate. The MFC was inoculated with municipal wastewater from the grit chamber effluent, which passes a primary sedimentation tank (primary clarifier). The MFC pilot plant including the peripheral devices is depicted in Figure 2.

Used analytics and models

The cell voltage (U_{MFC} in V) across the adjusted external electrical load resistance (R_{load} in Ω) of each electrical circuit (MFC-1 to 6) was continuously recorded with a controlling and monitoring unit (C&M unit; AWITE Bioenergie GmbH, Germany).

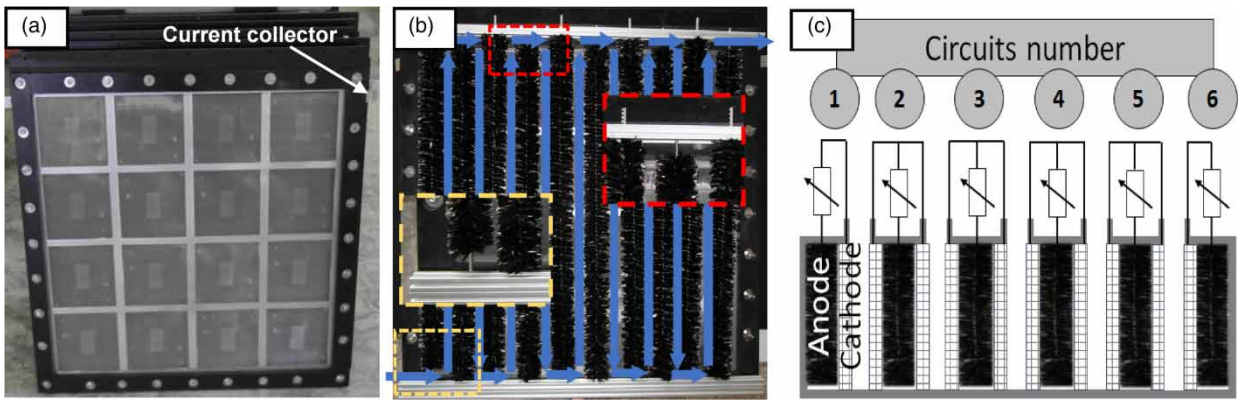

Figure 1 | (a) Large-scale raster segmented air-cathodes; (b) submersible electrode module with 10-graphite-brush assembly for cascade-like throughflow passage in flow direction; (c) sketch of five submerged modules (10 cathodes) and 6 anodes assembles across the direction of flow.

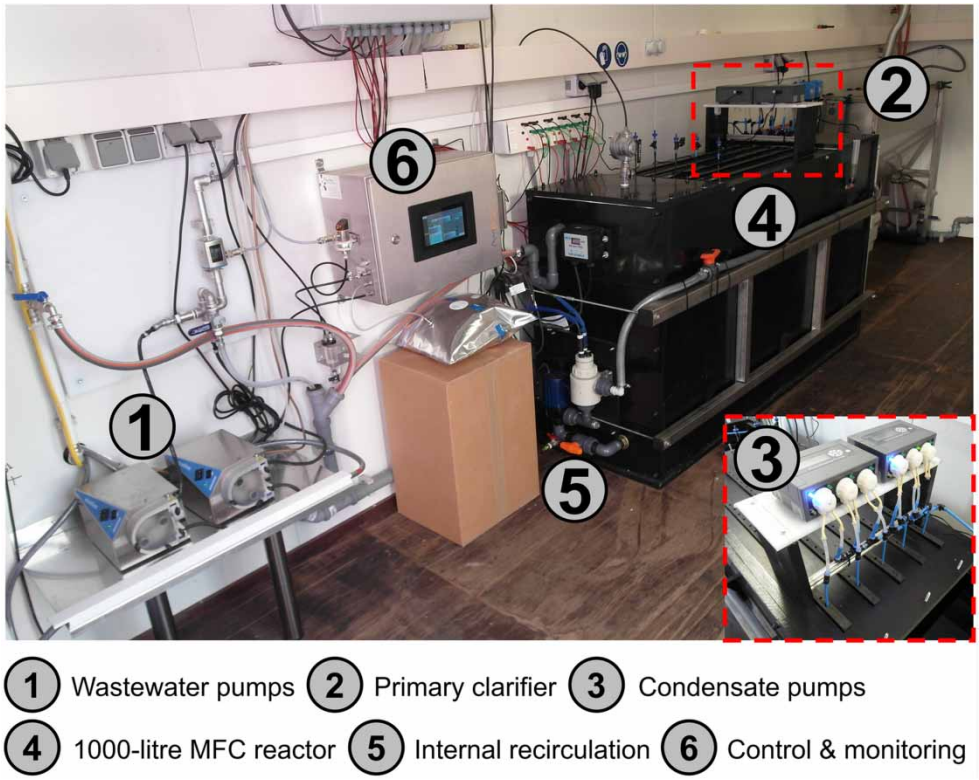

Figure 2 | On-site MFC pilot plant including the peripheral devices.

The C&M unit was equipped with a digital potentiometer and provided a resistor variation range from 0.5 to 50 Ω with a time interval of 1 min between resistor changes and a perturbation, ΔR_{load}, of 0.5 Ω (50–30 Ω), 0.3 Ω (30–10 Ω), and 0.1 Ω (10–0.5 Ω). Thus, the duration to record the polarisation curves was set to approximately 3 h and 20 min. For real-time optimisation, the P/O algorithm introduced by Woodward *et al.* (2010) was used to adjust the external resistance to react immediately to changes in operating conditions. Thus, each MFC was operated at its maximum power point. Before installation, the implemented P/O algorithm was verified on bench-scale single-chamber MFCs described elsewhere (Littfinski *et al.* 2021b). The flow rate was set to follow an empirical, typical diurnal pattern and was automatically controlled via the C&M unit. Accordingly, the mean hydraulic retention time (HRT) was 11 h (Days: 0–39) and 20 h (Days: 39–180), respectively. During rainfall events, the diurnal pattern was maintained. Rainfall events were only monitored in terms of reduced wastewater concentration and respective EC. Furthermore, the C&M unit was equipped with diverse sensors to monitor and record the actual bulk-liquid temperature, pH (pH + T; SE 101-MS, Knick, Germany), and EC (SE 615, Knick, Germany). Physically, the sensors were placed in a flow-through fitting of the internal recirculation of the reactor. Influent and effluent of volumetric proportional wastewater samples were analysed twice per week for the COD (LCK 114, LCK 314, LCK 1414, Hach, Germany), total nitrogen (TN; LCK 238, LCK 338, Hach, Germany), nitrite (NO_2^-; LCK 341, Hach, Germany), nitrate (NO_3^-; LCK 339, Hach, Germany), TAN (LCK 302, LCK 303, Hach, Germany), and BOD_{10} (biological oxygen demand) (Hach Lange BOD Direct).

With the exception of the dissolved inert fraction, all other COD fractionation measurements were carried out in the inlet and outlet of the pilot plant. To distinguish between dissolved and particulate, the samples were filtered through 0.45 μm filters according to the DWA-A 131 (2016). Hence, the COD was divided into a dissolved fraction (S) and a particulate fraction (X). Both fractions were further broken down into a biodegradable fraction (s) and an inert fraction (i) (Figure 3).

The dissolved inert fraction S_i was estimated based on filtrated COD samples of the effluent ($S_{COD,\ eff}$) from the secondary clarifiers (DWA-A 131 2016) of the WWTP Hecklingen (aerobic stabilisation). For the differentiation of the particulate fractions, long-term BOD measurements over 10 days were carried out respirometrically, considering the intermediate result for each day of the test duration. Using the model of a first-order degradation reaction, the limit value for the BOD_∞ was

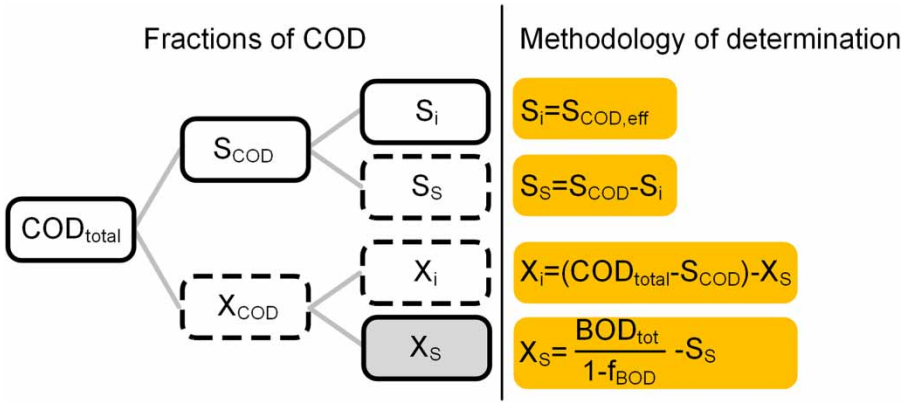

Figure 3 | COD fractionation and the methodology of its determination applied to the wastewater stream in- and outside the reactor. (Continuous line – directly measured; dotted line – calculated; grey shaded – calculated from BOD_{10} measurements).

determined by fitting the k-exponent with the method of least squares for each BOD_{10} test. For the final calculation of the total degradable substrate concentration BOD_{tot} ($S_S + X_S$), an additional fraction of 0.15 (f_{BOD}) was considered for the biomass formed to include the share used for cell growth (Roeleveld & Loosdrecht 2002; Gillot & Choubert 2010).

The pollutant treatment efficiency (η_{eli} in %) for COD, TN, and TAN (sum of ammonium and free ammonia nitrogen) is given by the following equation:

$$\eta_{eli} = \left(1 - \frac{C_{in}}{C_{eff}}\right) \times 100\ \% \tag{1}$$

where C_{in} (mg L^{-1}) and C_{eff} (mg L^{-1}) are the influent and effluent concentrations of a specific pollutant (COD, TN, or TAN).

The generated electrical current, I_{MFC} (in A), was estimated based on Ohm's law ($I_{MFC} = U_{MFC}/R_{load}$). Power ($PD_{Cat}$ in W m_{Cat}^{-2}) and current densities (j_{Cat} in A m_{Cat}^{-2}) were normalised to the cathode surface area (A_{Cat}; Circuits 1 and 6: 0.515 m_{Cat}^2; Circuits 2–5: 1.031 m_{Cat}^2) and calculated with $PD_{Cat} = U_{MFC}^2/(R_{load} \cdot A_{Cat})$ and $j_{Cat} = I_{MFC}/(R_{load} \cdot A_{Cat})$.

Theoretical power density curves (Equation (2)) were calculated based on an equivalent electrical circuit model approach that only considered the total internal (R_{Int} in Ω) and external load resistance in series. Using this simplified model, the polarisation curve becomes a straight line with a corresponding bell-shaped power density curve (Logan *et al.* 2018).

$$PD_{Calc} = \frac{U_{OCV}^2 \cdot R_{load}}{A_{Cat} \cdot (R_{Int} + R_{load})^2} \tag{2}$$

where PD_{Calc} is the theoretical power density (W m_{Cat}^{-2}); U_{OCV} is the open-circuit voltage (V); A_{Cat} is the cathode surface area (m^2), R_{load} is the external electrical load resistance (Ω), and R_{Int} is the overall internal resistance of the system (Ω).

The total internal resistance of each MFC was estimated based on the slope of the recorded polarisation curve ($R_{Int} = \Delta U_{MFC}/\Delta I_{MFC}$) by using the measured data points near the maximum power point. For a more advanced electrochemical analysis of the system, for the first time, the pulse-width modulated electrical load resistance (R-PWM) technique (Littfinski *et al.* 2021b) was applied to the pilot-scale MFC. The ohmic resistance was calculated from the immediate voltage transient response of the MFCs caused by switching frequencies of the external electrical circuit (from open-circuit to closed-circuit or vice versa) of 100 Hz (duty cycle: 80%).

The Coulombic efficiency (CE in %) and the normalised energy recovery per removed amount of COD (NER_{COD} in kWh_{el} $kg_{COD,deg.}^{-1}$) for a continuous-flow regime under steady-state conditions is calculated as:

$$CE = \frac{M_{O_2} \cdot I_{MFC}}{F \cdot b \cdot Q \cdot \Delta COD} \tag{3}$$

$$NER = \frac{\bar{P}}{\Delta COD \cdot Q} \tag{4}$$

where I_{MFC} is the electrical current (A), M_{O_2} is the molar weight of oxygen (32 g mol^{-1}); F is the Faraday constant (96,485 C mol^{-1}); b is the number of electrons changed per mole of oxygen (4); Q is the volumetric flow rate (L d^{-1}); ΔCOD is the difference between influent and effluent COD (mg$_{COD}$ L^{-1}); and $\bar{P}$ is the mean power (kW).

RESULTS AND DISCUSSION

Continuous operation performance

After a start-up phase of 15 days, the maximum power and current generated by the five submergible MFC modules reached 0.57 W (113 mW m_{Cat}^{-2}; normalised by a cathode area of 5.15 m_{Cat}^2) with a corresponding electrical current of 2.60 A (0.51 A m_{Cat}^{-2}; normalised by a cathode area of 5.15 m_{Cat}^2). The relatively high maximum power density (see Table 1) might be due to the high conductivity of the wastewater lowering the internal, or more specifically, the ohmic resistance. In the following period, an ongoing decrease in the overall MFC performance was observed, even though the conductivity and temperature did not change significantly. After 2 months of operation, the power generated by the reactor was only 20% of the maximum attainable power. Figure 4 shows the MFC performance during the different operation stages. Stage I

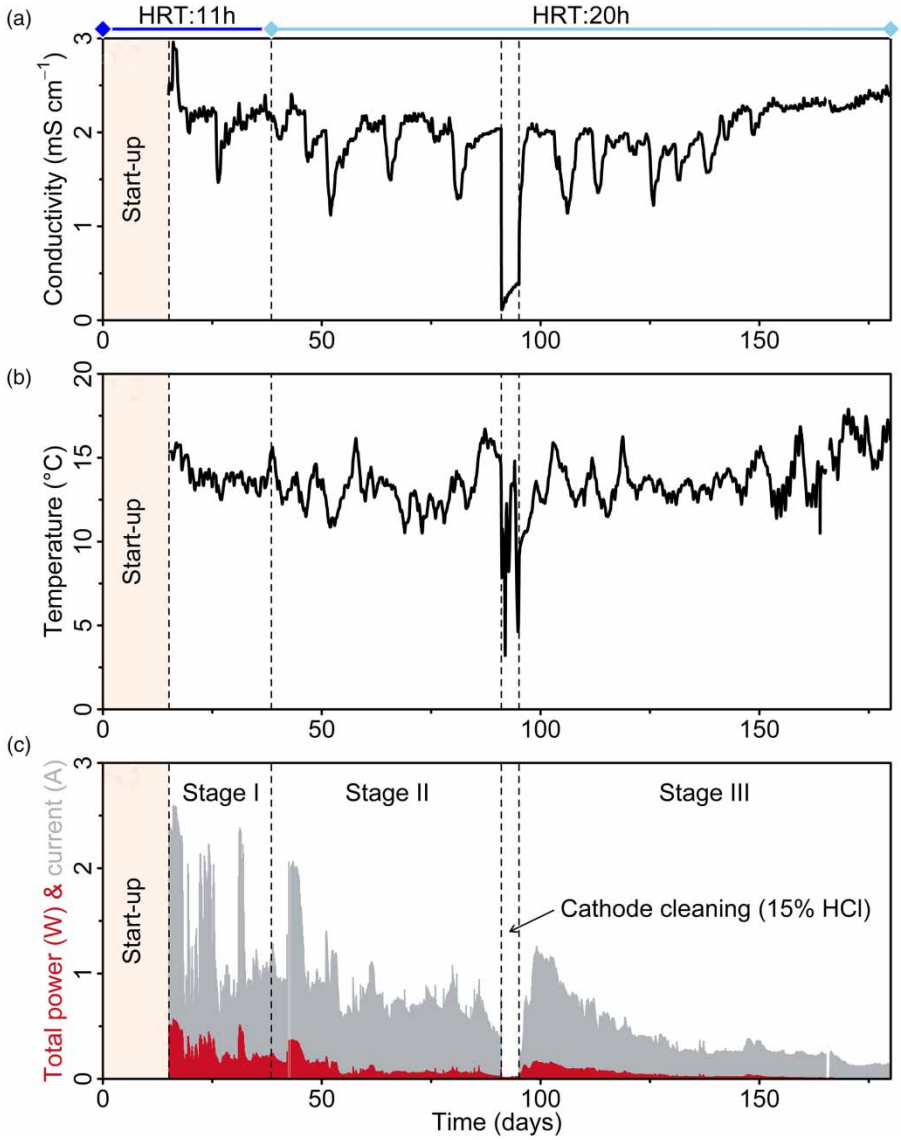

Figure 4 | Evolution of (a) EC within the reactor, (b) bulk-liquid temperature within the reactor, and (c) total power and electrical current during continuous operation with real municipal wastewater at a HRT of 11 h (Days: 0–39) and 20 h (Days: 39–180) in daily average.

represents the period of high wastewater inflow after start-up. Stage II is the ongoing operation with a reduced wastewater inflow, while Stage III represents the operation after a chemical cleaning of the cathode with 15% hydrochloric acid.

The hardly stable, measurable TN and TAN removal efficiencies (see Table 2) are caused by several factors mainly related to the cathodic conversion processes: (i) small specific cathode surface area (A_{Cat}/V_{MFC}) required for both nitrification and ammonia volatilisation, (ii) insufficient gas exchange inside the gas-filled inner chamber of the cathode resulting in gaseous ammonia accumulation and oxygen depletion, (iii) operational conditions (low temperature, low TAN concentration), (iv) insufficient current density to increase the pH near the cathode surface, (v) HRT of wastewater, and (vi) ongoing salt precipitation (presented below) leading to a reduced mass transfer. Nonetheless, chemical analysis of the accumulated – almost clear – water on the air-facing side of the gas diffusion cathode could provide indications regarding possible ammonia stripping. Results revealed that the pH and TAN concentrations of 9.7 and 68 $mg_{NH4\text{-}N}\ L^{-1}$, respectively, were far above the anolyte level (7.2 and 40 $mg_{NH4\text{-}N}\ L^{-1}$).

In contrast to the nitrogen elimination, the COD elimination was significant and constant throughout the operating time. Together with the low CE, this indicates the presence of additional non-exoelectrogenic microbial consortia such as heterotrophs and methanogens that are not influenced by electricity generation (Littfinski *et al.* 2022). Lower CE in Stage I compared to that in Stages II and III might be a result of the shorter HRT, which leads to a higher organic loading rate. The correlation between CE and organic loading rate was also reported by Choi & Ahn (2013), who observed a nearly exponential decrease in CE with an increasing organic loading rate due to microbial side reactions consuming COD without releasing current.

COD fractionation

Due to the used methodology of COD determination presented above, S_i is constant for the MFC influent and effluent. The elimination of all other fractions could be observed. The total elimination rate of COD is composed of the slightly lower retention rate of X_i and the slightly higher degradation rates for X_S and S_S (see Figure 5). No COD measurements were performed

Table 2 | Operational data and performance evaluation parameter of the 1,000-litre single-chamber MFC

	Stage I	Stage II	Stage III
Operational data			
Day of operation	Days 15–39	Days 39–91	Days 95–180[a]
HRT in h	11	20	20
$T_{bulk\text{-}liquid}$ in °C	14.0 ± 0.8	13.2 ± 1.3	13.9 ± 1.5
$EC_{bulk\text{-}liquid}$ in mS cm^{-1}	2.2 ± 0.2	1.9 ± 0.2	2.0 ± 0.3
$pH_{bulk\text{-}liquid}$	7.2 ± 0.1	7.0 ± 0.3	7.1 ± 0.3
COD_{in} in $mg_{COD}\ L^{-1}$	299 ± 88	285 ± 43	266 ± 65
TN_{in} in $mg_{N}\ L^{-1}$	64 ± 5	57 ± 8	53 ± 8
TAN_{in} in $mg_{N}\ L^{-1}$	35 ± 5	35 ± 5	30 ± 8
Energetic parameter			
max. PD_{Cat} in mW m_{Cat}^{-2}	113 ± 6	74 ± 15	34.0 ± 17.2
max. j_{Cat} in mA m_{Cat}^{-2}	531 ± 106	422 ± 90	224 ± 35
$R_{P/O}$ in Ω (MFC-1 and 6)	1.5 ± 0.7	1.0 ± 0.3	2.4 ± 1.0
$R_{P/O}$ in Ω (MFC-2 to 5)	1.1 ± 0.5	0.6 ± 0.2	1.3 ± 0.5
CE in %	1.6 ± 0.7	7.2 ± 3.6	5.0 ± 3.1
NER_{COD} in $kWh_{elec.}\ kg_{COD,deg.}^{-1}$	0.025 ± 0.012	0.039 ± 0.024	0.024 ± 0.026
Pollutant treatment efficiency			
$\eta_{COD,eli}$ in %	34 ± 8	34 ± 4	33 ± 7
$\eta_{TN,eli}$ in %	13 ± 6	5 ± 10	7 ± 9
$\eta_{TAN,eli}$ in %	4 ± 9	4 ± 8	−4 ± 11

[a]After cathode cleaning with HCl between operation days 91 to 95.

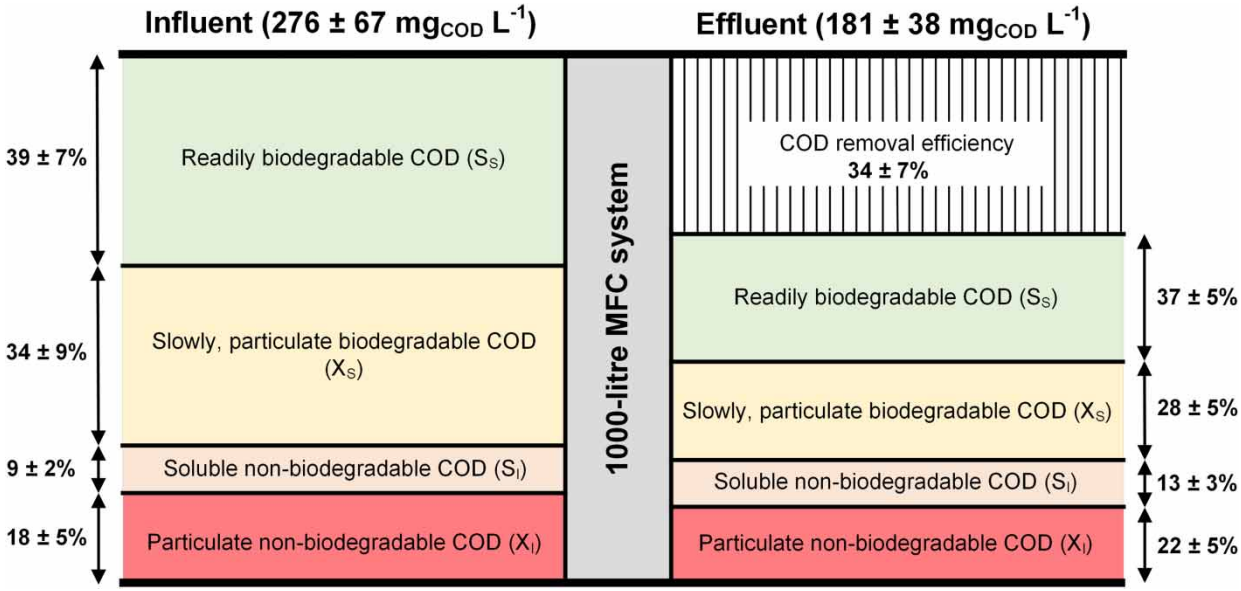

Figure 5 | Average measured COD fractions for the influent and effluent of the 1,000-L MFC reactor during the presented 6-month period of operation.

for the formation of sludge found on the anodes, cathodes, or at the bottom of the reactor. Consequently, additional tests on the residual particulate matter in the biofilm and reactor are necessary.

Reactor performance during rainfall events

A short-time fluctuation in electricity generation was observed during rainfall events and is a result of dilution effects, i.e. decrease in EC and substrate limitation. To investigate dilution effects, polarisation curves were recorded on two consecutive days without a rainfall event (Day 16, 2.9 mS cm^{-1}) and during a rainfall event (Day 18, 2.3 mS cm^{-1}). The rainfall event significantly decrease the maximum power density by 51% (MFC-1 and 6) and 53% (MFC-2 to 5) compared to that on Day 16. Corresponding to the reduced power output, the mean total internal resistance tripled from 0.56 $\pm$ 0.02 Ω (MFC-1 and 6) and 0.39 $\pm$ 0.02 Ω (MFC-2 to 5) at Day 16 to 1.72 $\pm$ 0.04 Ω (MFC-1 and 6) and 1.21 $\pm$ 0.07 Ω (MFC-2 to 5) at Day 18. Due to the unexpectedly low internal resistance (<0.5 Ω), the recorded polarisation curve (no rainfall event) almost stopped near the maximum power point. Hence, to complete the power density curves, the evolution of these curves at higher current densities was predicted using the presented simplified model (Equation (2)). As depicted in Figure 6, the model was able to successfully predict the evolution of the power density curves for each MFC on Days 16 and 18. Nevertheless, the simplified equivalent electrical circuit model does not consider capacitive effects. Figure 6 also illustrates that the measured maximum power density for MFC-1 and 6 was higher than that of MFC-2 to 5. MFC-2 to 5 had one anode assembly sharing two cathodes, while the similar anode assembly of MFC-1 and 6 had only one cathode to discharge. In accordance with Zhao & Chen (2018), the fast stepwise resistor reduction leads to capacitive electrical currents of the anode, overestimating the power density compared to the equilibrium state. The capacitive current (in combination with the faradaic current) can cause the higher power density for MFC-1 and 6 measured with the simultaneous resistor reduction rate on MFC-2 to 5.

Since the observed power density curve followed the bell-shaped function, it can be assumed that the non-linear activation and concentration losses are dominated by ohmic losses. The ohmic resistance was almost the same for each MFC and was on average 0.61 $\pm$ 0.05 Ω (2.2 mS cm^{-1}). Using the total internal resistance determined on Day 18 as a reference (same EC), the degree of contribution of the ohmic resistance to the overall internal resistance was 35% (MFC-1 and 6) and 51% (MFC-2 to 5), respectively (see Figure 7). Hence, the remaining 65 and 49% of overall internal resistance can be assigned to activation, concentration, and turnover kinetic losses.

Different from the direct and immediate power response of the system, the load resistance reacts with a lag in time (hysteresis). The load resistance set by the P/O algorithm hardly increased simultaneously with the decreasing conductivity (see Figure 8) even with an adaption rate of 0.1 Ω per minute. With a delay of several hours, the external resistance regulated itself incrementally to the expected higher level. In the following decline of the rainwater influence with an accompanying

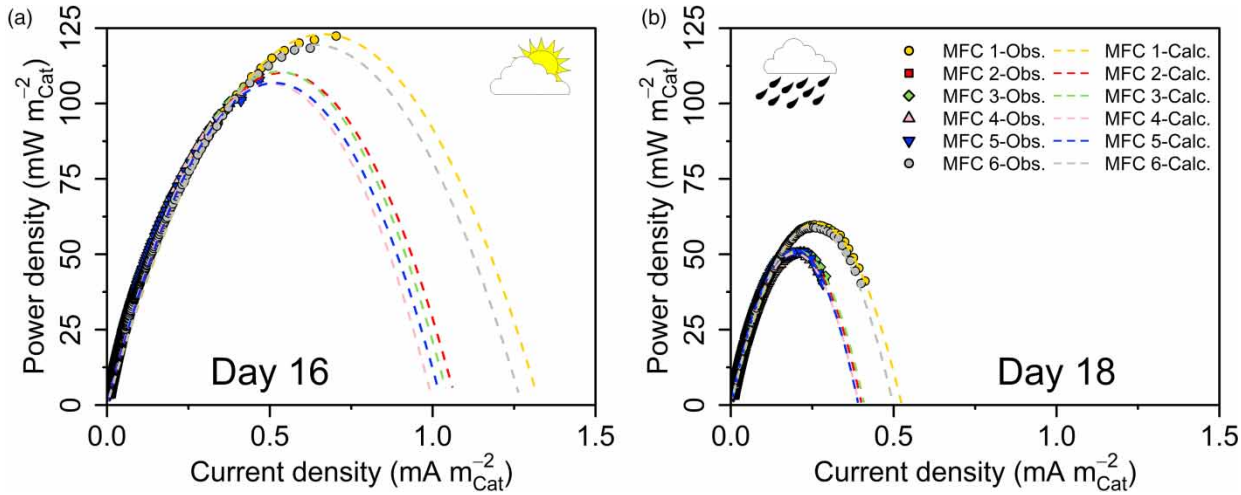

Figure 6 | Measured and calculated power density curves normalised to the cathode surface area (MFC-1 and 6: 0.515 m^2_{Cat} and 1.57 m^2_{An}; MFC-2 to 5: 1.031 m^2_{Cat} and 1.57 m^2_{An}). Power density curves were recorded for (a) a dry and (b) a rainy day.

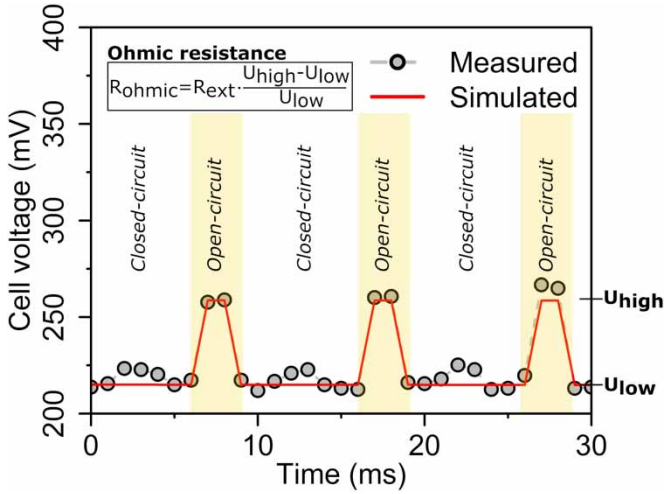

Figure 7 | Ohmic resistance estimation based on the voltage response induced by the R-PWM technique (100 Hz; duty cycle of 80%), a representative for MFC-5. R_{ext} is the external resistance in Ohm, adjusted by MPPT, U_{high} and U_{low} are the results of the R-PWM measurement in V.

increase of the conductivity, the resistance regulation remained at this higher level or even continued to increase. After several hours, the settings were adjusted to the lower resistance close to the starting conditions.

A clear and direct correlation between conductivity and resistance control only by ohmic resistance can therefore be excluded. A separate recording of the individual losses (activation-, ohmic-, concentration-related) was not carried out continuously. The interpretation of the influence of concentration gradients, biofilm adaptions, capacitive effects, etc., even in the diurnal cycle of the municipal WWTP, was therefore difficult.

Figure 8 shows the influence of the cathode area, providing the exchange surface for diffusive mass transport and determining the diffusive losses. Consequently, a lower total resistance R was achieved by the P/O algorithm for the 1.03 m^2 cathode area modules compared to the 0.515 m^2 cathodes (see Table 2).

Salt precipitation and cathode regeneration

The observed long-term performance reduction (see Figure 4(c)) is mainly associated with cathode contaminations. In general, two major mechanisms can contribute to internal and surface cathode contamination: (i) biofilm formation on the water-

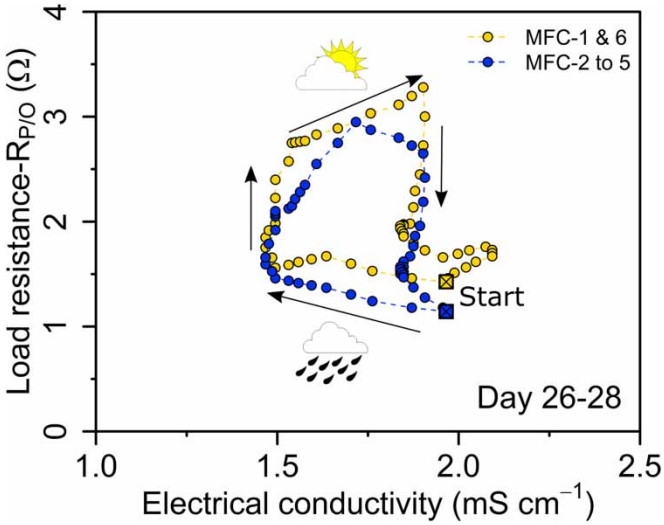

Figure 8 | Hysteresis effects of the load resistance adjusted by the P/O algorithm because of dilution effects during a rain event. Each shown data point is with a time difference of 1 h.

facing side of the cathode and (ii) inorganic scaling as a result of salt deposits on the catalyst and the gas diffusion layer. Biofilms, especially when using separators on the cathode, function as a diffusion barrier, reducing the mass ion transport to the cathode interface. Salt crystallisation in the meso- and micropores of the catalyst layer reduces the reactive three-phase interface.

The chemical analysis of the catholyte at the air-facing side of the cathode showed an acid capacity ($K_{S,4.3}$) of 70.4 mmol L^{-1}, which was approximately six times higher than that of the anolyte. Using the chemical equilibrium model *Visual MINTEQ 3.1* (https://vminteq.lwr.kth.se/download/), the composition of potential salt deposits was predicted, which included calcite, $CaCO_3$, hydroxyapatite, $Ca_5(PO_4)_3OH$ and dolomite, $CaMg(CO_3)_2$, for the wastewater composition and temperature. These potential deposits correspond to the high acid capacity, which is mainly defined by the hydrogen carbonates of calcium, magnesium, and sodium. According to the thermodynamic calculations, dolomite might be the dominating deposit (60 and 100% of the calcium and magnesium fractions, respectively) when assuming a pH of >9 near the cathode surface. Since dolomite dissolves quite slowly in acid, the short reaction time (<180 min) with HCl (15% solution) during the chemical cleaning procedure explains the incomplete recovery of MFC performance after the chemical treatment (Days 91–95). Figure 9 shows the observed deposits in the cathodes after removing the glass fibre separator and brushing the biofilm off with water.

CONCLUSIONS

One of the world's largest air-cathode MFC systems (1,000 L) equipped with five submergible multi-electrode modules was operated at a municipal WWTP over a 6-month period. The system, fed with mechanically treated wastewater, generated a maximum power of 0.57 W (2.60 A) or 113 mW m_{Cat}^{-2}, at a current density of 0.51 A m_{Cat}^{-2}. The COD removal efficiency of the flow reactor was 34% ($T = 14$ °C). In addition to the reduction of biodegradable COD, in average, 20% of the particulate inert material was also retained from the wastewater stream. The distribution of the different COD fractions due to bio-electrochemical wastewater treatment was subject to only minor changes. Nevertheless, the elimination rate of 34 ± 7% COD, in particular, 41 ± 10 mg L^{-1} of the readily biodegradable fraction, results in a reduced EBPR or upstream denitrification rate. In contrast, the nitrogen removal efficiency (13 ± 6% during operation Stage I at 14 °C) proved to be volatile, mainly caused by cathode-limiting processes. If it can be stabilised, the envisaged application scenario appears to be possible upstream of an activated sludge tank, without affecting TN effluent limits. The technology was able to demonstrate its ability to regenerate after rain events. The reduced loads to the activated sludge stage may result in potential savings in terms of energy

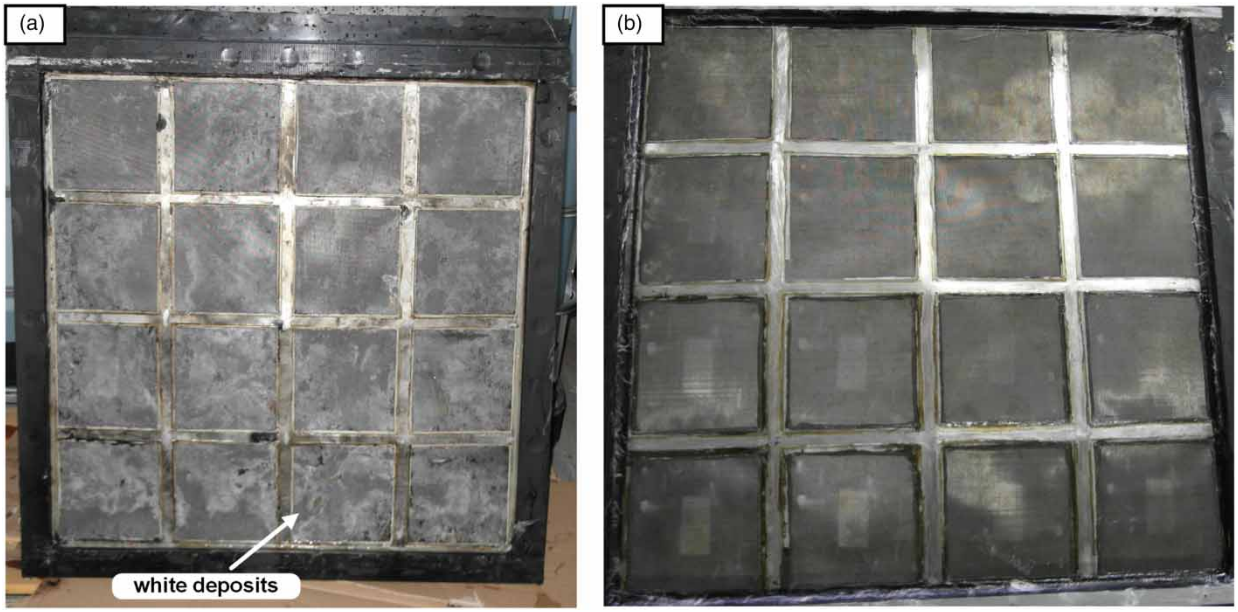

Figure 9 | (a) Excessive formation of white salt deposits below the removed glass fibre layer on the catalytically active side of the air-cathodes after 91 days of operation. (b) Cathode after mechanical and chemical cleaning using a 15% HCl solution.

consumption and (excess) sludge quantities. In addition to the stabilisation of nitrogen decomposition, the full-scale application of the MFC technology still essentially depends on the long-term stability of the process, which is currently limited by the deposition of salts and biofilm formation in the electrocatalytic structure of the used air-cathode with activated carbon catalyst. Accordingly, further investigations are still required concerning applicable materials and methods of operation.

ACKNOWLEDGEMENTS

The authors of this work gratefully acknowledge the financial support of the German Federal Ministry of Education and Research (BMBF), funding code: 02WQ1466A-C, and the project support provided by the Project Management Agency Karlsruhe (PTKA).

DATA AVAILABILITY STATEMENT

All relevant data are included in the paper or its Supplementary Information.

CONFLICT OF INTEREST

The authors declare there is no conflict.

REFERENCES

Adekunle, A., Raghavan, V. & Tartakovsky, B. 2019 Real-time performance optimization and diagnostics during long-term operation of a solid anolyte microbial fuel cell biobattery. *Batteries* **5**, 9.

Babanova, S., Jones, J., Phadke, S., Lu, M., Angulo, C., Garcia, J., Carpenter, K., Cortese, R., Chen, S., Phan, T. & Bretschger, O. 2020 Continuous flow, large-scale, microbial fuel cell system for the sustained treatment of swine waste. *Water Environment Research* **92** (1), 60–72.

Bird, H., Heidrich, E. S., Leicester, D. D. & Theodosiou, P. 2022 Pilot-scale microbial fuel cells (MFCs): a meta-analysis study to inform full-scale design principles for optimum wastewater treatment. *Journal of Cleaner Production* **346**, 131227.

Choi, J. & Ahn, Y. 2013 Continuous electricity generation in stacked air cathode microbial fuel cell treating domestic wastewater. *Journal of Environmental Management* **130**, 146–152.

DWA-A 131 2016 *Bemessung von Einstufigen Belebungsanlagen*. DWA Deutsche Vereinigung für Wasserwirtschaft, Abwasser und Abfall e.V, Hennef, Germany.

Feng, Y., Yang, Q., Wang, X. & Logan, B. E. 2010 Treatment of carbon fiber brush anodes for improving power generation in air–cathode microbial fuel cells. *Journal of Power Sources* **195** (7), 1841–1844.

Gillot, S. & Choubert, J.-M. 2010 Biodegradable organic matter in domestic wastewaters: comparison of selected fractionation techniques. *Water Science & Technology* **62** (3), 630–639.

Harnisch, F. & Schröder, U. 2010 From MFC to MXC: chemical and biological cathodes and their potential for microbial bioelectrochemical systems. *Chemical Society Reviews* **39** (11), 4433.

Hiegemann, H., Herzer, D., Nettmann, E., Lübken, M., Schulte, P., Schmelz, K.-G., Gredigk-Hoffmann, S. & Wichern, M. 2016 An integrated 45 L pilot microbial fuel cell system at a full-scale wastewater treatment plant. *Bioresource Technology* **218**, 115–122.

Hiegemann, H., Littfinski, T., Krimmler, S., Lübken, M., Klein, D., Schmelz, K.-G., Ooms, K., Pant, D. & Wichern, M. 2019 Performance and inorganic fouling of a submergible 255 L prototype microbial fuel cell module during continuous long-term operation with real municipal wastewater under practical conditions. *Bioresource Technology* **294**, 122227.

Hille, A., He, M., Ochmann, C., Neu, T. R. & Horn, H. 2009 Application of two component biodegradable carriers in a particle-fixed biofilm airlift suspension reactor: development and structure of biofilms. *Bioprocess and Biosystems Engineering* **32**, 31–39.

Littfinski, T., Beckmann, J., Gehring, T., Stricker, M., Nettmann, E., Krimmler, S., Murnleitner, E., Lübken, M., Pant, D. & Wichern, M. 2021a Model-based identification of biological and pH gradient driven removal pathways of total ammonia nitrogen in single-chamber microbial fuel cells. *Chemical Engineering Journal* **431**, 133987.

Littfinski, T., Nettmann, E., Gehring, T., Krimmler, S., Heinrichmeier, J., Murnleitner, E., Lübken, M., Pant, D. & Wichern, M. 2021b A comparative study of different electrochemical methods to determine cell internal parameters of microbial fuel cells. *Journal of Power Sources* **494**, 229707.

Littfinski, T., Stricker, M., Nettmann, E., Gehring, T., Hiegemann, H., Krimmler, S., Lübken, M., Pant, D. & Wichern, M. 2022 A generalized whole-cell model for wastewater-fed microbial fuel cells. *Applied Energy* **321**, 119324.

Logan, B. E. 2008 *Microbial Fuel Cells*. John Wiley & Sons, Hoboken, NJ, USA.

Logan, B. E., Zikmund, E., Yang, W., Rossi, R., Kim, K.-Y., Saikaly, P. E. & Zhang, F. 2018 Impact of ohmic resistance on measured electrode potentials and maximum power production in microbial fuel cells. *Environmental Science & Technology* **52** (15), 8977–8985.

Roeleveld, P. J. & Loosdrecht, M. C. M. v. 2002 Experience with guidelines for wastewater characterization in The Netherlands. *Water Science & Technology* **45** (6), 77–87.

Rossi, R., Wang, X., Yang, W. & Logan, B. E. 2019a Impact of cleaning procedures on restoring cathode performance for microbial fuel cells treating domestic wastewater. *Bioresource Technology* **290**, 121759.

Rossi, R., Jones, D., Myung, J., Zikmund, E., Yang, W., Gallego, Y. A., Pant, D., Evans, P. J., Page, M. A., Cropek, D. M. & Logan, B. E. 2019b Evaluating a multi-panel air cathode through electrochemical and biotic tests. *Water Research* **148**, 51–59.

Rossi, R., Hur, A. Y., Page, M. A., Thomas, A. O., Butkiewicz, J. J., Jones, D. W., Baek, G., Saikaly, P. E., Cropek, D. M. & Logan, B. E. 2022 Pilot scale microbial fuel cells using air cathodes for producing electricity while treating wastewater. *Water Research* **215**, 118208.

Tan, W. H., Chong, S., Fang, H.-W., Pan, K.-L., Mohamad, M., Lim, J. W., Tiong, T. J., Chan, Y. J., Huang, C.-M. & Yang, T. C.-K. 2021 Microbial fuel cell technology – a critical review on scale-up issues. *Processes* **9**, 985. https://doi.org/10.3390/pr9060985.

Wang, Z. & He, Z. 2020 Demystifying terms for understanding bioelectrochemical systems towards sustainable wastewater treatment. *Current Opinion in Electrochemistry* **19**, 14–19.

Woodward, L., Perrier, M., Srinivasan, B., Pinto, R. P. & Tartakovsky, B. 2010 Comparison of real-time methods for maximizing power output in microbial fuel cells. *AIChE Journal* **56** (10), 2742–2750.

Zhao, W. & Chen, S. 2018 Critical parameters selection in polarization behavior analysis of microbial fuel cells. *Bioresource Technology Reports* **3**, 185–190. doi:10.1016/j.biteb.2018.07.010.

First received 8 December 2022; accepted in revised form 25 March 2023. Available online 6 April 2023